RSC Advances

PAPER

View Article Online
View Journal | View Issue

Cite this: *RSC Adv.*, 2021, **11**, 29215

Effects of graphene oxide size on curing kinetics of epoxy resin

Xuebing Chen,[a] Weijiao Jiang,[a] Bo Hu,[b] Zhiming Liang,[b] Yue Zhang,*[b] Jian Kang,*[a] Ya Cao[a] and Ming Xiang[a]

To study the effects of graphene oxide (GO) size on the curing kinetics of epoxy resin (EP), two kinds of GO were selected and characterized by Fourier transform infrared spectrometry (FT-IR), FT-Raman spectrometry (FTIR-Raman), thermo gravimetric analysis (TGA), dynamic light scattering (DLS), transmission electron microscopy (TEM), X-ray diffractometry (XRD) and X-ray photoelectron spectroscopy (XPS). The results showed that the two kinds of GO had similar chemical structures but different sizes—the average particle size of GO-A was 190.1 nm and that of GO-B was 1510 nm, and GO-A has more oxidizing groups on its surface. The two kinds of GO were separately added to EP, and the curing kinetics of GO/EP composites and neat EP were investigated through differential scanning calorimetry (DSC). It can be seen that the addition of GO promoted the curing process of the EP system, and GO-A had a more significant catalytic effect. Furthermore, the curing activation energy (E_a) was calculated by Kissinger model, and the change of E_a in the whole curing reaction process was studied by Ozawa method to further understand the curing mechanism. It showed that the apparent E_a of EP system increases with the increase of the conversion rate, and E_a of EP-A is obviously lower in the early curing stage. However, as the curing reaction proceeds, E_a of EP-B is a little lower than that of EP-A in the later curing stage. But EP-A has the lowest E_a combined with the whole process from Kissinger method. To sum up, it can be concluded that the curing process of EP can be promoted by adding GO and the smaller size (190.1 nm) of GO had a greater effect and lower E_a than the GO with particle size of 1510 nm. And the related mechanisms were discussed and analyzed.

Received 7th July 2021
Accepted 22nd August 2021

DOI: 10.1039/d1ra05234a

rsc.li/rsc-advances

1 Introduction

Epoxy Resin (EP) is one of the most frequently used matrix resins because of its low price, high adhesion, outstanding chemical and heat resistance, and excellent mechanical and electrical insulation properties.[1–3] It has been widely used in many fields of industry, such as engineering adhesives, coatings, semiconductor encapsulation, hardware components, electronic circuit board materials, and components of automotive, marine, and aerospace composite materials.[4–7]

However, EP also has the undesirable property of brittleness with low fracture resistance and poor electrical conductivity because of their structure, which limits their applications in some fields.[8] In recent years, the enhancement of EP by adding nanofillers has been widely reported, such as nano-silica, nano clay, carbon nanotubes, carbon black, and fullerene.[2,9] Compared with traditional fillers, nanofillers can effectively improve the properties of EP.[10–12] As anatomically thick, two-dimensional substance with a high aspect ratio (width to thickness), superior mechanical, thermal, and electrical properties, graphene oxide (GO) becomes an excellent nanofiller for the production of high strength, high thermal and electrically conductive polymer nanocomposites.[12–15]

There has been much research about the GO/EP composites. Research results demonstrated that the properties of EP depend a lot on the influence of nanofillers on the curing behavior of EP. And by using non-isothermal crystallization kinetics, the effect of GO on the non-isothermal curing behavior of the EP system was investigated. Hu *et al.* studied the effect of imidazole-modified GO on curing kinetics of an EP system containing 1.5% phosphorus. Li *et al.*[16] prepared surface amine-rich functionalized GO by amination reaction and studied its effect on curing kinetics of EP. Ryu *et al.*[17] studied and compared the curing kinetics of hexamethylenediamine functionalized GO/EP system and the original GO/EP system, and determined the relevant curing kinetics parameters by the Kissinger method and the Friedman method. Kuilla *et al.*[18] studied the influence of GO on the cure behavior with four different heating rates. From the references above, it can be concluded that the filler of GO can affect the curing rate, the formation of crosslinking structure, glass transition

[a]*State Key Laboratory of Polymer Materials Engineering, Polymer Research Institute of Sichuan University, Chengdu 610065, China*

[b]*Dongfang Electric Machinery Co., Ltd., Deyang, 618000 China. E-mail: metaspark@163.com*

temperature and curing temperature, and curing activation energy (E_a) of the EP system. Furthermore, the curing kinetics can be changed after the addition of nanofiller into EP system, thus affecting the material properties of EP. Some studies also investigated the effect of GO content on curing kinetics, but some of the conclusions are inconsistent, indicating that the research on this system is not full-fledged.

The studies above mainly focus on the effect of the modification and content of GO on the EP system. However, the shape and particle size also influence the curing kinetics. J. Abenojar *et al.*[19] studied the curing process, wear behavior, and mechanical properties of an epoxy adhesive filled with two different particle sizes of boron carbide (B_4C), respectively. The result showed that the B_4C particle size affects the curing rate. Zhao *et al.*[20] discussed the influence of glass beads content and size on the kinetic parameters and found smaller filler size had lower E_a and a faster curing speed at the beginning of the curing reaction. Such studies about the effect of nanofiller particle size on the curing kinetic are not full-fledged enough, and few people have studied the effect of GO particle size on curing reaction kinetics of EP system. Also, the theoretical study of curing mechanism is also not clear. To better understand the impact of GO on EP system and choose the most appropriate GO size, it is essential to study effects of GO size on curing kinetics of EP, which is also con tributes to determining the processing technology, reaction condition and formulation production of composites.[21,22]

In our study, different curing kinetics models such as Kissinger and Ozawa method were used to study the non-isothermal curing kinetics of GO/EP, and the effect of GO size on the curing process of EP was discussed. All of these studies above provided a theoretical basis for the determination of the curing process of GO/EP composites.

2 Experimental

2.1 Materials

The bisphenol-A epoxy resin (industrial pure, grade E51, epoxy equivalent 184–195 g mol^{-1}) was purchased from Deyuan Chemical Co., Ltd., China. Two kinds of GO (GO-A, GO-B) were kindly provided by Deyangene Carbon Technology Co., Ltd., China. The amine curing agent (JH-0422, amine value 750–850 mg KOH g^{-1}) was purchased from Changshu Jiafa Chemical Co., Ltd., China.

The chemical structures of E51, GO and JH-0422 are shown in Fig. 1.

2.2 Preparation of GO/EP composites

0.02 g of GO (GO-A and GO-B) and 400 mL of ethanol were added to a beaker, and ultrasound for 2 hours. Then 4 g of EP was added and ultrasound for 2 hours. After that, the solution was stirred at 90 °C for 12 hours to evaporate the ethanol, and vacuumed in a 90 °C vacuum oven for 2 hours to remove the remaining ethanol. Then, the amine curing agent of JH-0422 with a mass fraction of 20% was added to the system and stirred until a homogeneous mixing system was obtained, and the samples (EP-A and EP-B) required for the test were obtained.

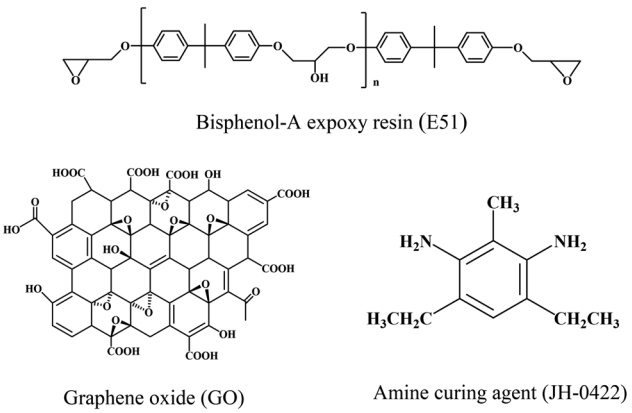

Fig. 1 Structure of EP, GO and JH-0422.

2.3 Characterization and measurement

The spectra of GO-A and GO-B were recorded by Fourier transform infrared spectrometer (FT-IR, PerkinElmer Frontier, PerkinElmer Corp., USA) under transmission mode. The scanning range was 4000–400 cm^{-1}, the accuracy was 4 cm^{-1}, and the scanning times were 16 times; the chemical structure and composition of GO sample surface were analyzed by X-ray Photoelectron Spectroscopy (XPS, Thermo Scientific K-Alpha, Thermofisher, USA). The test conditions were vacuum degree of 5×10^{-9} mbar, monochromatic Alka source (Mono Alka), the energy of 1486.6 eV, the voltage of 15 kV, beam current of 15 mA, scanning mode of the analyzer of CAE, and the instrument work function of 4.2.[23–26]

The X-ray Diffractometry (XRD) patterns of GO-A and GO-B were obtained through a diffractor (Ultima IV, Rigaku Corp., Japan). The wavelength of Cu Kα radiation was $\lambda = 0.154$ nm and the scanning rate was 10° min^{-1}. For GO-A and GO-B, powder samples were used and spectra were recorded in the range of 2θ = 0–90°.[27–30]

The molecular structure of GO can be further analyzed by FT-Raman Spectrometer (FTIR-Raman, Renishaw inVia, Bruker Corp., England). The wavelength of the laser is 514 nanometers; Thermo Gravimetric Analysis (TGA, FG 209 F1, Netzsch Corp., Germany) test was conducted to analyze the oxygen-containing functional group content of GO-A and GO-B. About 2 mg of GO powder was weighed and placed in a crucible under a nitrogen atmosphere at a heating rate of 10 °C min^{-1}. And the temperature range was from 30 °C to 800 °C; GO particle sizes dissolved in DI H_2O were measured by Dynamic Light-Scattering (DLS) using a Malvern instrument particle size analyzer (Zetasizer Nano-ZS, Malvern Corp., UK). Scattering was measured at an angle of 173°. The GO samples were diluted with DI H_2O to a concentration of 1 mg mL; to further analyze the structure and observe the size of GO-A and GO-B, Transmission Electron Microscopy (TEM, Tecnai G2 F20 S-TWIN, FEI, USA) was performed under an accelerating voltage of 200 kV. The TEM sample was dispersed in ethanol and deposited on a copper grid

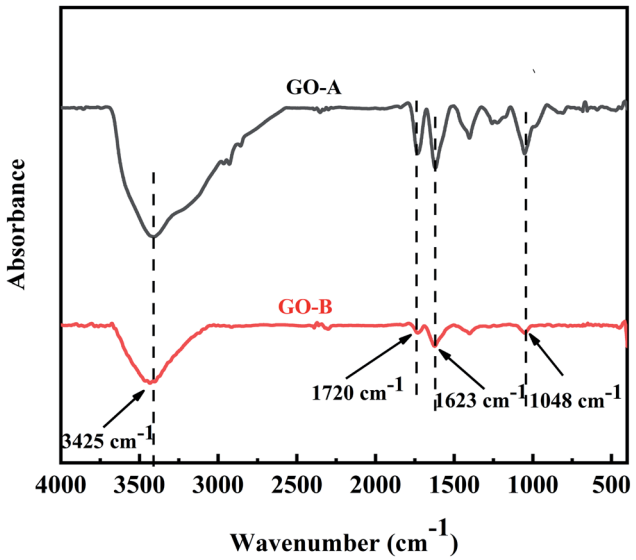

Fig. 2 Infrared spectra of GO-A and GO-B.

for observation; Scanning Electron Microscope (SEM, ZEISS Gemini 300, Carl Zeiss AG, Germany) was performed for GO/EP composites to observe distribution of the GO particles in the EP. Before measurements, impact fracture surfaces of the samples were coated with gold.[31,32]

All non-isothermal curing reaction experiments were performed with Differential Scanning Calorimeter (DSC, DSC1, Mettler Toledo, Switzerland) under continuous nitrogen flow of 50 mL min^{-1}. The standard procedure for each experiment was the following: 5–8 mg of sample was weighted, heated to 300 °C at different heating rates, *i.e.* 5 °C min^{-1}, 10 °C min^{-1}, 15 °C min^{-1}, and 20 °C min^{-1}, to analyze the cure behavior.[33–36]

3 Results and discussion

3.1 Characterization

3.1.1 Characterization of GO-A and GO-B. In this section, the chemical structures, morphologies and particle sizes of GO-A and GO-B were characterized by FTIR, XPS, XRD, Raman, TGA and TEM.

The FT-IR spectra result of two kinds of GO is shown in Fig. 2, and the absorption peaks are clearly observed. Besides, the peaks at 1048 cm^{-1}, 1623 cm^{-1}, 1720 cm^{-1}, and 3425 cm^{-1} are relevant with C–O–C stretching, C=C stretching, C=O stretching and –OH stretching, respectively, which correspond to the characteristic groups of GO. It can be seen that GO-A and GO-B have the same peak emergence location, indicating that they have the same chemical structure.

The chemical structure and composition of GO-A and GO-B surfaces were analyzed by XPS. According to Fig. 3(a), O1s, C1s, and N1s are the main element signal peaks and the amount of the elements are similar. Also, Fig. 3(b) and (c) are

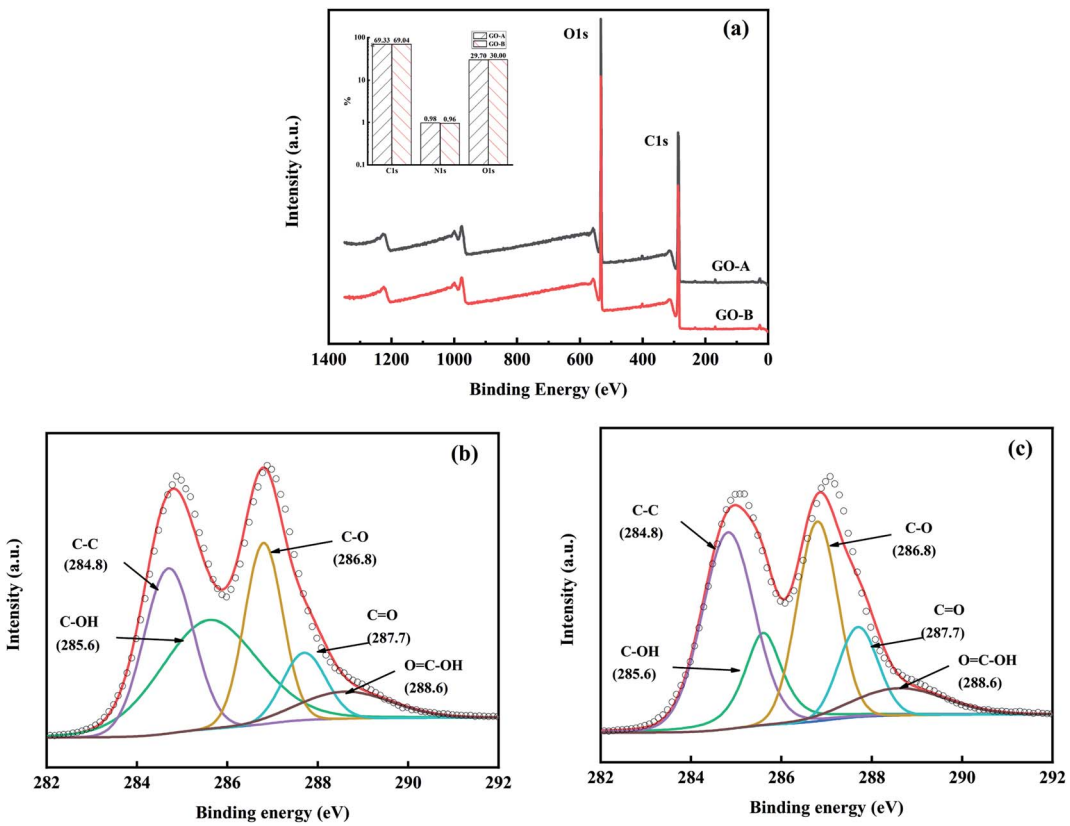

Fig. 3 XPS survey spectrum (a), curve fitting of C1s spectra of the GO-A (b) and GO-B (c).

Table 1 Proportions of various carbon bonds for the GO-A and GO-B

Sample	C–OH (%)	C–C (%)	C–O (%)	C=O (%)	O=C–OH (%)
GO-A	18.9	34.9	29.6	7.2	9.3
GO-B	16.0	36.2	26.8	15.0	5.9

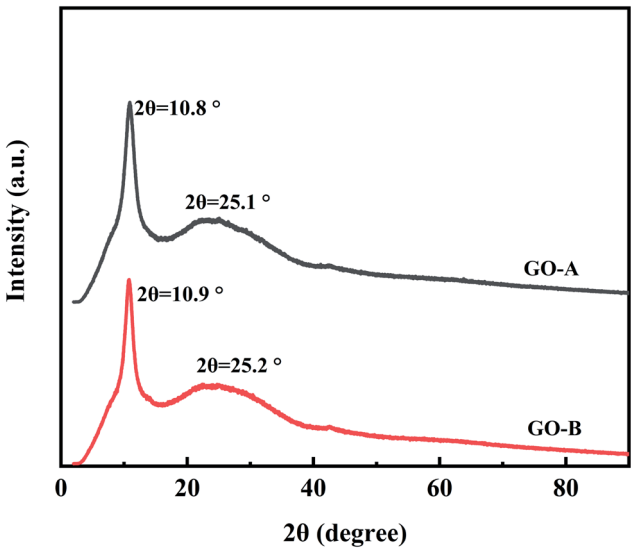

Fig. 4 XRD patterns of GO-A and GO-B.

curve fitting of C1s spectra of the GO-A and GO-B, and the proportions of various carbon bonds are shown in Table 1. It can be seen that the C1s spectrum can be fitted by five Gaussian–Lorentzian peaks including C–C (284.8 eV), C–OH (285.6 eV), C–O (286.8 eV), C=O (287.7 eV), and C=C–OH (288.6 eV). It can be found that GO-A and GO-B contain a large number of oxygen-containing groups such as hydroxyl and

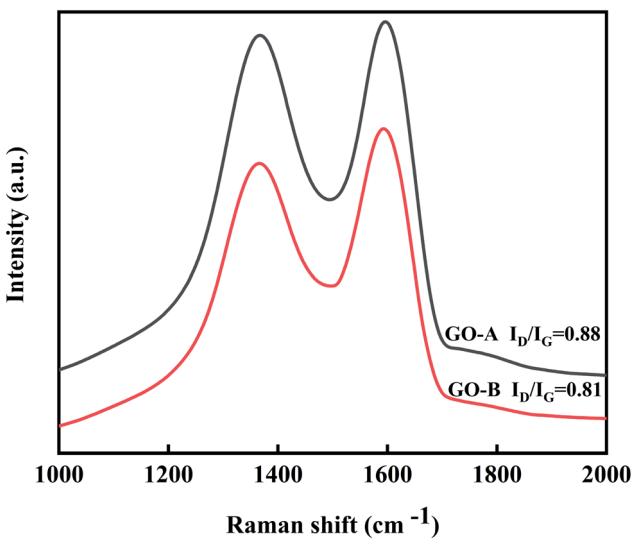

Fig. 5 Raman spectra of GO-A and GO-B.

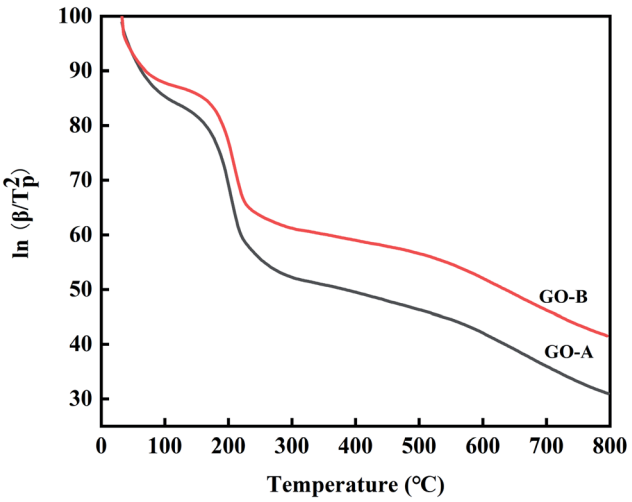

Fig. 6 TGA curves of the GO-A and GO-B.

carboxyl groups, and the content of hydroxyl and carboxyl groups in GO-A is obviously higher than that in GO-B.[37,38]

Fig. 4 is the XRD pattern of the two kinds of GO. In the spectrum, the intensive sharp peak for the (001) plane of GO is shown at about $2\theta = 10°$ and the broad peak for the (002) plane of graphene is observed at about $2\theta = 25°$. Based on the Bragg's law, the layer spacing of GO-A and GO-B can be calculated as 0.82 nm and 0.81 nm, respectively. And it indicates that the size difference of GO does not change its composition and structure.[39]

Fig. 5 is the Raman spectra of GO-A and GO-B. For GO, the D-band (1360 cm^{-1}), which represents an atomic lattice defect caused by the disordered vibrations of C–C, results from the sp^3 hybridized part. And the G-band (1600 cm^{-1}), which is caused by the C=C stretching vibration in the plane, is the sp^2 hybrid part. Therefore, the ratio of I_D/I_G indicates the extent of surface defects in GO. By calculating, the I_D/I_G of GO-A is greater than

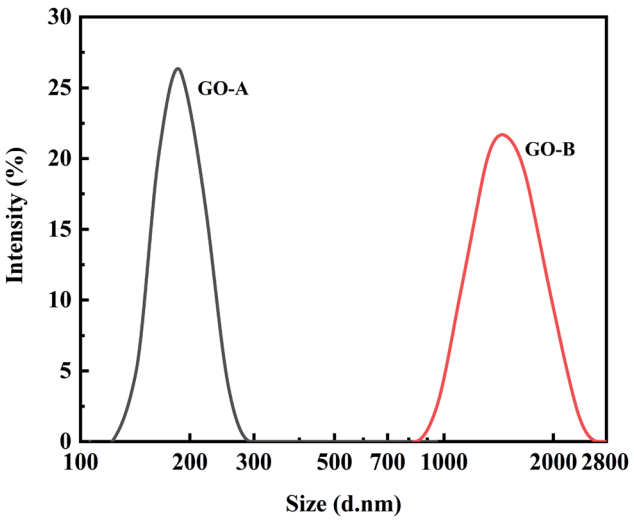

Fig. 7 The particle size distribution of GO-A and GO-B.

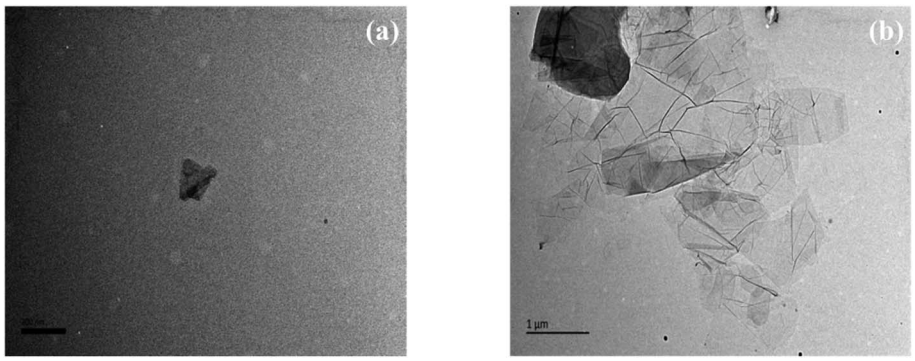

Fig. 8 TEM images of GO-A (a) and GO-B (b).

that of GO-B, which indicates that the GO-A surface has more defects and oxygen-containing groups.

Fig. 6 is TGA curves of the GO-A and GO-B. The first phase of losing weight is below 100 °C. This results from a large number of oxygen-containing functional groups in GO. They absorb water molecules in the air, and the free water and bound water evaporate when the temperature is raised. The second stage of weightlessness at about 200 °C is caused by the decomposition and gasification of a large number of oxygen-containing functional groups on the GO surface and the gasification of some of the water combined with the oxygen-containing functional groups. Then, due to numerous defects on the GO surface, the third stage begins to lose weight at around 500 °C. It can be calculated that the weightlessness of GO-A in the first and second paragraphs is approximately 14.9% and 35.1%, and that of GO-B is about 11.5% and 28.5%. The result shows GO-A absorbs more water and has more oxygen-containing functional groups.

The particle sizes of GO-A and GO-B were determined by DLS and TEM. For both samples, the particle size distributions were observed by DLS with the average particle sizes of 191.10 nm and 1510 nm, which is shown in Fig. 7. Besides, TEM images may give a more realistic insight into the particle sizes. Although the bending, overlapping, and shape differences may affect the observation of particle size distribution, it can be seen clearly from TEM images presented in Fig. 8 that the particle size of GO-B is much larger than that of GO-A. Meanwhile, both of them have a certain degree of irregular stacking and aggregation, and there are many small folds as well as fragments randomly arranged together at the edge of GO lamellae.

3.1.2 Characterization of GO/EP composites. Fig. 9 shows the cryogenically fractured surface SEM images of EP-A

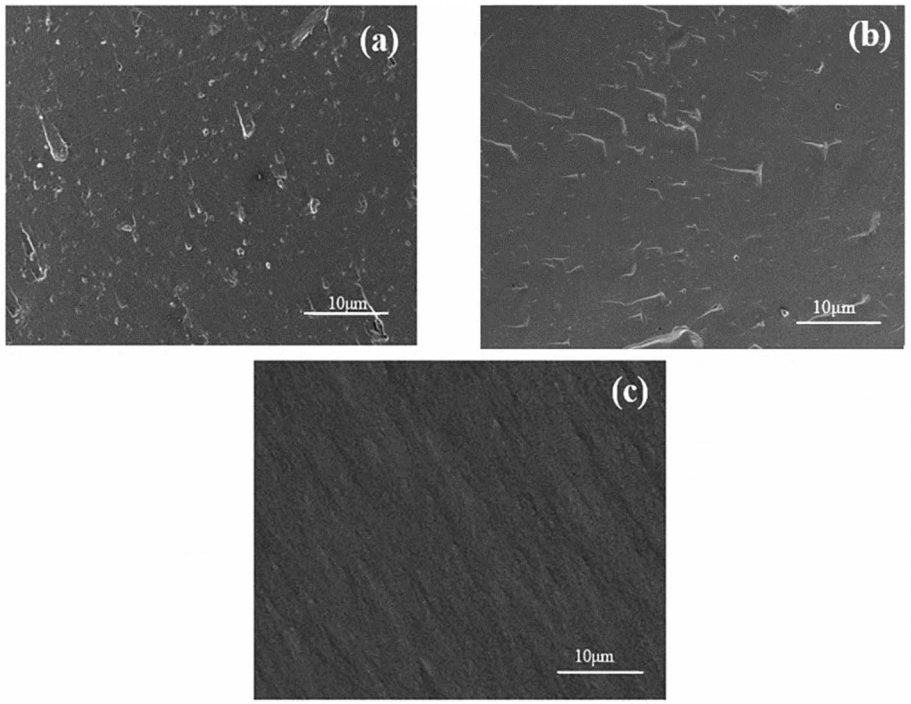

Fig. 9 SEM images of the cryogenically fractured surface morphologies of GO-A/EP (a), GO-B/EP (b), and neat EP (c), respectively.

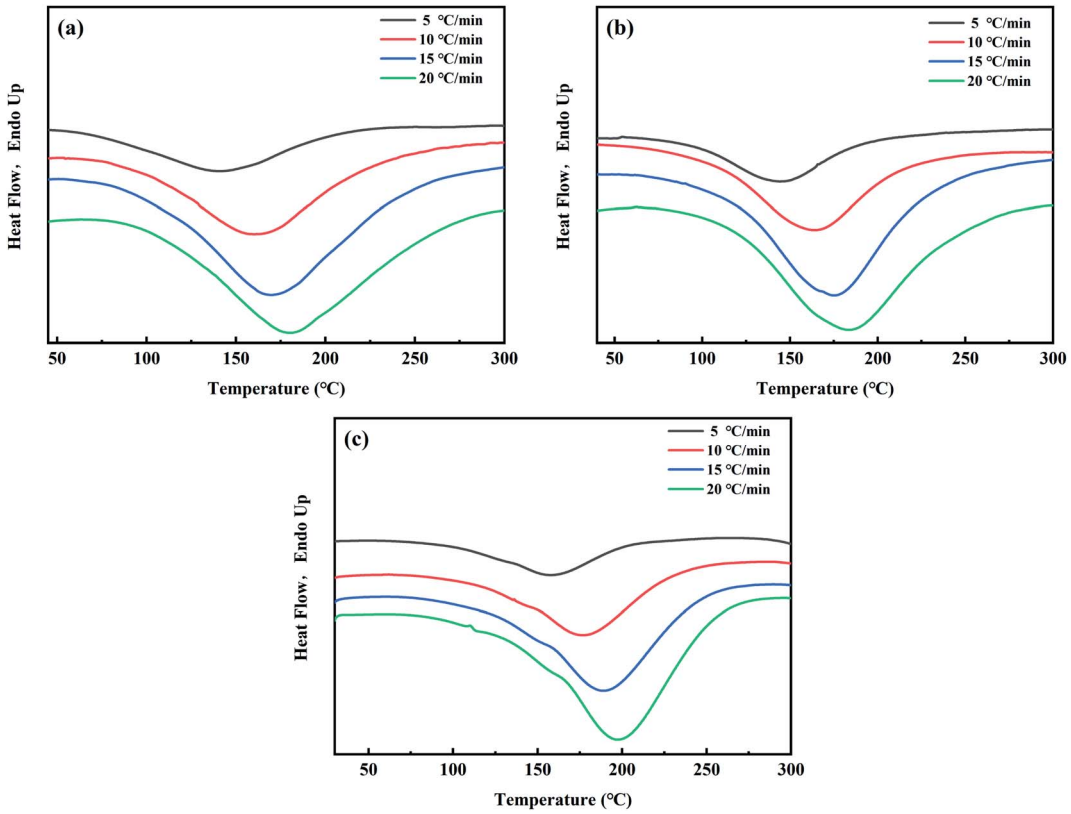

Fig. 10 DSC curves of EP-A (a), EP-B (b) and neat EP (c) at different heating rates.

composites, EP-B composites and neat EP. From Fig. 9, it can be seen that the cross section morphology of the epoxy composite changes greatly after the addition of GO, and some uniformly distributed fracture structures appear. Although it is difficult to directly attribute these morphologies to the fillers, the presence of these relatively uniformed fracture surface patterns indicate the fine dispersion of GO in the matrix.[40–42]

3.2 Curing kinetics analysis

The curing process of GO/EP is complex and affects the material properties, so the curing kinetics analysis is contributed to studying the properties and curing conditions of the EP system, and provides theoretical guidance and basis for the molding and manufacturing of the GO/EP composite materials. Therefore, non-isothermal DSC was used to test the key curing kinetic parameters.

Fig. 10 shows the non-isothermal DSC curves of enthalpy *versus* temperature of EP-A, EP-B, and neat EP at the heating rates of 5 °C min^{-1}, 10 °C min^{-1}, 15 °C min^{-1}, and 20 °C min^{-1}, respectively. And Table 2 shows the curing peak temperatures (T_p) of the epoxy curing reactions at different heating rates obtained from Fig. 10.

It can be seen from Fig. 10 that the rate of total enthalpy change gradually increases to the maximum as the curing reaction proceeds at the beginning, and then decreases after the peak temperature. It reveals that at the beginning of the curing process, the chain lengths are increasing, and the rate of total enthalpy change is increasing. However, as the reaction goes on and the crosslinking begins, the rate of total enthalpy change gradually decreases until the end of curing process. In addition, it can be seen from Fig. 10 and Table 2 that compared with neat EP, T_p of EP-A and EP-B all decrease by about 15 °C. The addition of GO significantly promotes the curing process of EP, and T_p of EP-B is about 3 °C higher than that of EP-A, indicating that GO-A has a more significant catalytic effect on the curing process.

Studies have demonstrated that compounds containing hydroxyl groups can promote the reaction between EP and amines or other nucleophiles.[43] Therefore, epoxy groups

Table 2 T_p values for EP-A, EP-B and neat EP from the DSC measurements at different heating rates

Sample	β (°C min^{-1})	T_p (°C)
EP-A	5	141.2
	10	160.8
	15	172.8
	20	180.0
EP-B	5	144.0
	10	163.5
	15	175.4
	20	183.0
Neat EP	5	158.0
	10	177.3
	15	189.0
	20	197.7

become more vulnerable to nucleophiles. Due to the constant generation of hydroxyl groups in the reaction process, the curing reaction between EP and amines has autocatalytic characteristics in the initial reaction stage.[44] The different types of oxidizing groups on the GO surface have similar catalytic properties to the hydroxyl groups generated in the curing process of epoxy, facilitating the curing reaction of EP with amine curing agents.

Fig. 11 shows the curve of conversion rate (α) *versus* the temperature of EP-A, EP-B and neat EP at the different heating rates of 5 °C min^{-1}, 10 °C min^{-1}, 15 °C min^{-1}, and 20 °C min^{-1}, respectively. α represents the degree of reaction at the particular temperature

$$\alpha = \frac{\Delta H_T}{\Delta H} \quad (1)$$

where ΔH_T is the reaction heat from the onset of polymerization up to temperature T, and ΔH is the total reaction heat. The conversion rate of each system shows an S-shaped curve with the temperature. That's to say, α increases regularly with the increase of T, which indicates that the system has the autocatalytic property,[44,45] and the curing mechanism of the EP system cannot be completely changed by the addition of GO. It can be seen that the curing degree of the system is low when the temperature is under 150 °C. Then the curing rate increases rapidly with the temperature, reaching a very high curing degree. During this period, EP goes through chain growth, branching, and self-crosslinking, which limits the movement of the molecules and slows the curing rate. Also, from Fig. 11(d), at the same temperature, EP-A has the highest degree of curing, while neat EP has the lowest degree, indicating that the addition of GO promotes the curing process and the promotion effect of GO-A was more obvious.

It can be concluded that GO-A with an average particle size of 190.1 nm promoted the curing process of the EP system more obviously than GO-B with average particle size of 1510 nm. This is because the surface of GO-A contains more oxidizing groups, which has a catalytic effect and accelerates the ring-opening reaction of EP.

In order to further understand the relationship between the curing rate of GO/EP system and temperature, mathematical differential treatment is performed on the curves in Fig. 11. And the T–dα/dT curves of EP-A, EP-B, and neat EP are obtained, as shown in Fig. 12. It can be seen from Fig. 12 that in the early curing stage, the curing rate increases with the increase of temperature. However, in the later stage, the curing rate gradually slows down, which is because the cross-linking occurs at the time and the system viscosity increases, making the reaction more difficult. As can be seen from Fig. 12(d), in the early curing stage, at the same temperature, EP-A has a higher curing rate, and the fastest to reach the peak curing rate. In the later stage, the curing rate is lower than EP-B and neat EP. This is because the early stage of reaction is mainly controlled by chemical reaction, and more active groups and reaction sites promote the

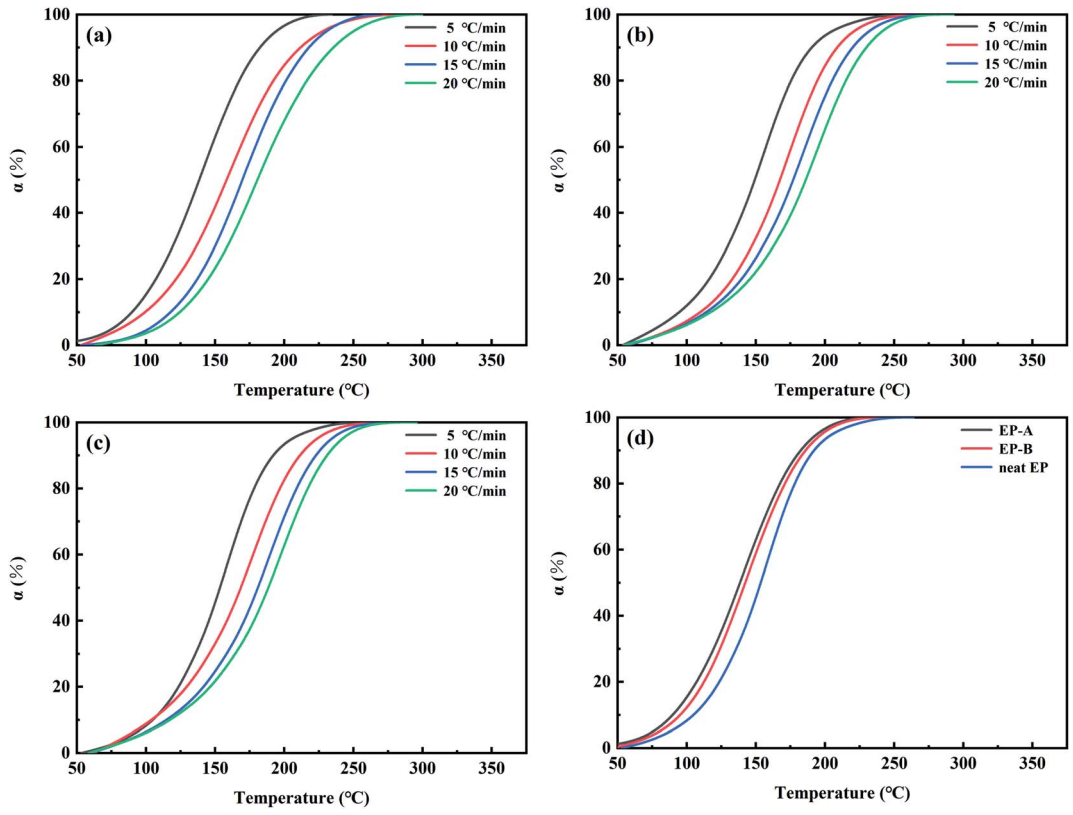

Fig. 11 The conversion rate α *versus* temperature of EP-A (a), EP-B (b) and neat EP (c) at different heating rates and temperature and (d) T–α diagram of EP-A, EP-B and neat EP at the heating rate of 5 °C min^{-1}.

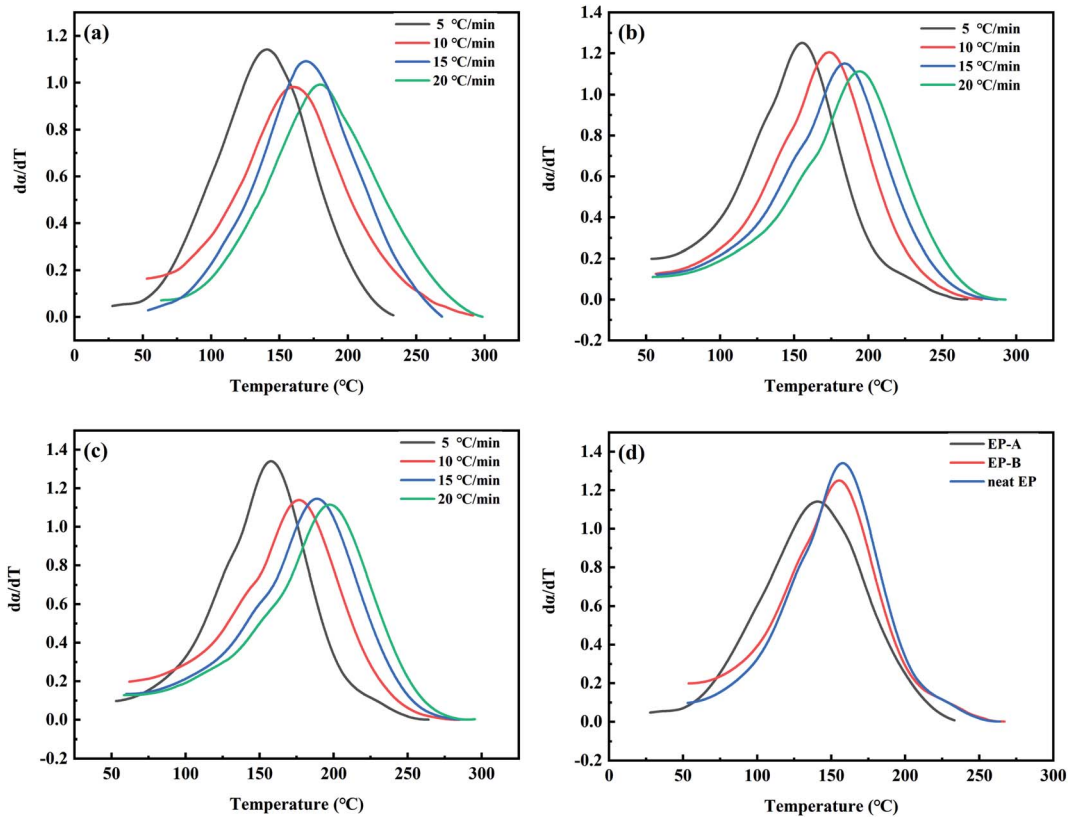

Fig. 12 The dα/dT *versus* temperature of EP-A (a), EP-B (b) and neat EP (c) at different heating rates and (d) T–dα/dT diagram of EP-A, EP-B and neat EP at heating rate of 5 °C min^{-1}.

curing reaction. However, in the later stage of reaction, the concentration of active group is greatly reduced, and the crosslinking network generated by curing limits the movement of molecules, and curing is gradually controlled by diffusion reaction. And GO blocks the molecules from moving. The larger particle size of GO, the bigger the hindering effect, but GO-A has more hindering sites at the same mass content, and a large number of sites will cooperate to restrict the movement of the reaction chain at a deeper level and larger range.[46]

3.3 Calculation of curing activation energy

3.3.1 Kissinger method. E_a is defined as the minimal energy required for a chemical reaction. To further study the catalytic behavior of GO in the EP curing process, E_a of EP-A, EP-B, and neat EP were calculated and compared. The calculation formula of the Kissinger method is as follows.[47–51]

$$\ln\left(\frac{\beta}{T_p^2}\right) = \ln\left(\frac{A \times R}{E_a}\right) - \frac{E_a}{R} \times \frac{1}{T_p}\Delta h_m^{\circ}(T_c) \quad (2)$$

E_a can be obtained from the slope of the line of $\ln(\beta/T_p^2)$–$1/T_p$.[49] Fig. 13 shows E_a calculated by the Kissinger method. E_a reflects the initial state of the non-isothermal curing reaction, and the methods are all based on the maximum reaction rate corresponding to the lowest point of the curve, *i.e.* T_p. According to Fig. 13 and eqn (2), E_a of EP-A, EP-B, and neat EP are 47 395.61 J mol^{-1}, 49 117.73 J mol^{-1}, and 51 445.95 J mol^{-1} respectively. It can be concluded that E_a of the EP system decreases after the addition of GO. Among them, E_a of EP-A decreases by about 7%, and that of EP-B goes down by about 4%.

3.3.2 Owaza method. The curing reaction of EP is a very complicated process, which includes multi-step chemical

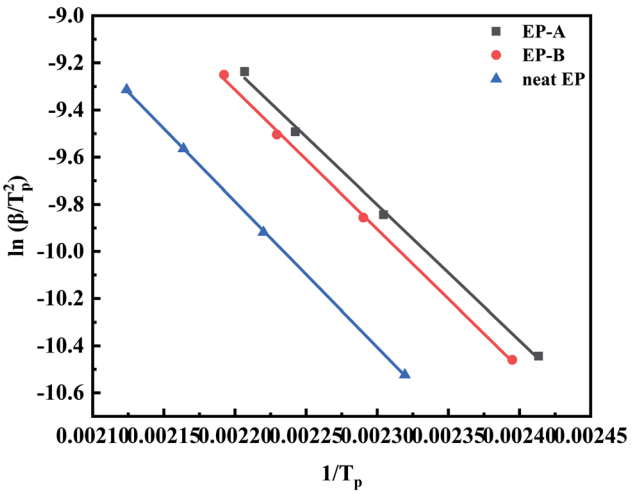

Fig. 13 The Kissinger plot of $\ln(\beta/T_p^2)$ *versus* $1000/T_p$ of EP-A, EP-B and neat EP.

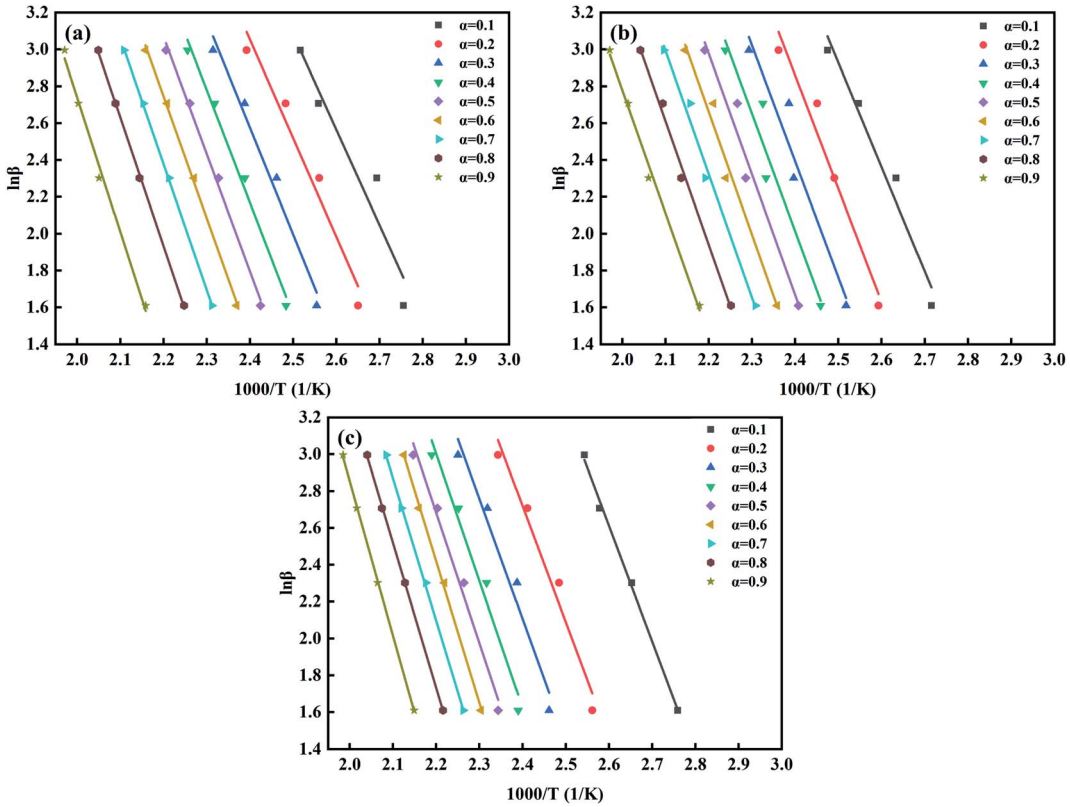

Fig. 14 The fitting plots of ln β *versus* 1000/T of EP-A (a), EP-B (b) and neat EP (c).

reactions and complex physical changes. During the whole curing reaction process, E_a of the system will change greatly. By studying the change of E_a, the main controlling factors in different reaction stages can be investigated, which helps to further understand the curing mechanism of the system and provide theoretical guidance for the study of curing kinetics. The apparent E_a at different conversion rates can be obtained by using Ozawa method.[52,53] The formula is as follows.

$$\frac{d[\ln(\beta)]}{d(1/T_p)} = -1.052\frac{E_a}{R} \quad (3)$$

At different heating rates, when the conversion rates are 90%, 80%, 70%, 60%, 50%, 40%, 30%, 20%, and 10%, the curves of ln β–1/T of the three kinds of composites are shown in Fig. 14. According to the slope in Fig. 14, the apparent E_a at the same conversion rate can be calculated, as shown in Fig. 15. It can be seen from Fig. 15 that the apparent E_a of EP increases with the increase of conversion rate. Possible mechanis has been proposed here: the polymerization of the EP system is complex and involves multiple reactions. In the early stage, when temperature is low, reaction mainly occurs between EP and primary amines and this reaction is most easy to occur. Also, a large number of –OH, –COOH, and other oxidizing groups on the GO surface further accelerates the curing reaction. The above factors give a low apparent E_a, and E_a of EP-A which has larger amount of oxidizing groups is lower than that of EP-B. In the later stage, when temperature is high, most primary amine is converted to secondary amine, making the reaction between secondary amine and EP becomes dominant.[2,54–57] And side reactions such as etherification or homopolymerization may occur.[58] So, the apparent E_a becomes higher. In addition, at the later stage, as the reactions go on, the viscosity increases and the active groups are consumed, the curing reaction is more diffusion-controlled. The larger the size of GO, the greater the hindrance effect on the diffusion

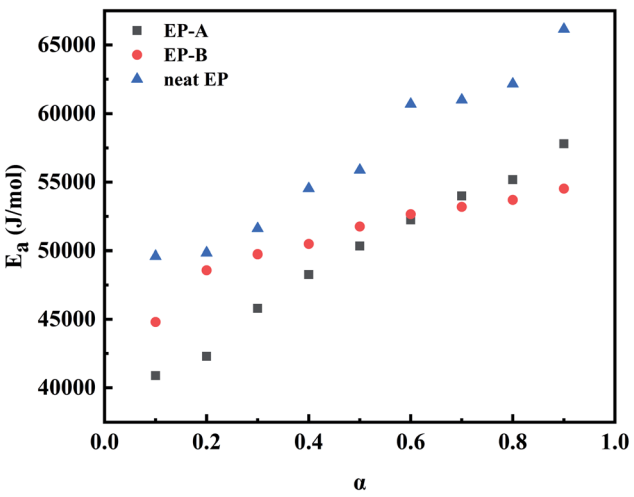

Fig. 15 Changes in E_α of EP-A, EP-B and neat EP curing as the function of conversion α.

movement of molecules. However, under the same mass content, GO-A has more hindrance sites, and a large number of sites will cooperate to restrict the movement of the reaction chain in a deeper and wider range.[16,46,58]

4 Conclusions

In this study, two kinds of GO whose average particle sizes are 190.1 nm (GO-A) and 1510 nm (GO-B) were separately added to EP for researching the effect of GO size on the curing kinetics of GO/EP composites by DSC test. Curing reactions including four different heating rates were investigated, and the curing kinetic parameters of the EP-A, EP-B and neat EP were obtained by Kissinger and Ozawa method. The results revealed that the addition of GO significantly promoted the curing process of EP. Both the half curing time and the curing temperature reduced, and T_p of EP-A was lower than that of EP-B. From the calculations of Kissinger and Ozawa method, the apparent E_a of EP system increases with the increase of conversion rate, and E_a of GO/EP is lower than neat EP in the overall curing process. And E_a of EP-A is much lower in the early curing stage. However, as the curing reaction proceeds, E_a of EP-B is a little lower in the later curing stage. But EP-A has the lowest E_a combined with the whole process from Kissinger method. From all the results above, it can be concluded that the addition of GO significantly promoted the curing process of EP, and on the whole, GO-A had a better catalytic effect on the curing process.

Conflicts of interest

There are no conflicts to declare.

Acknowledgements

We are grateful for financial support by National Natural Science Foundation of China (NSFC, Grant No. 51503134, 51702282) and State Key Laboratory of Polymer Materials Engineering (Grant No. SKLPME 2017-3-02), and the Analytical and Testing Center of Sichuan University for providing XPS, XRD and TEM measurement.

References

1 Z. Hao, L. Li, X. Liao, X. Sheng and Y. Zhang, Preparation and toughening performance investigation of epoxy resins containing carbon nanotubes modified with hyperbranched polyester, *Polym. Bull.*, 2018, **75**(3), 1013–1026.

2 L. Lu, L. Xia, H. Zengheng, S. Xingyue, Z. Yi and L. Pan, Investigation on cure kinetics of epoxy resin containing carbon nanotubes modified with hyper-branched polyester, *RSC Adv.*, 2018, **8**(52), 29830–29839.

3 T. Na, H. Jiang, L. Zhao and C. Zhao, Preparation and characterization of novel naphthyl epoxy resin containing 4-fluorobenzoyl side chains for low-k dielectrics application, *RSC Adv.*, 2017, **7**(85), 53970–53976.

4 S. Liu, H. Yan, Z. Fang, Z. Guo and H. Wang, Effect of graphene nanosheets and layered double hydroxides on the flame retardancy and thermal degradation of epoxy resin, *RSC Adv.*, 2014, **4**(36), 18652–18659.

5 I. Zaman, T. T. Phan, H.-C. Kuan, Q. Meng, L. T. B. La, L. Luong, O. Youssf and J. Ma, Epoxy/graphene platelets nanocomposites with two levels of interface strength, *Polymer*, 2011, **52**(7), 1603–1611.

6 C. Bao, Y. Guo, L. Song, Y. Kan, X. Qian and Y. Hu, In situ preparation of functionalized graphene oxide/epoxy nanocomposites with effective reinforcements, *J. Mater. Chem.*, 2011, **21**(35), 13290–13298.

7 S. Liu, V. S. Chevali, Z. Xu, D. Hui and H. Wang, A review of extending performance of epoxy resins using carbon nanomaterials, *Composites, Part B*, 2018, **136**, 197–214.

8 A. Reghunadhan, J. Datta, N. Kalarikkal, J. T. Haponiuk and S. Thomas, Toughness augmentation by fibrillation and yielding in nanostructured blends with recycled polyurethane as a modifier, *Appl. Surf. Sci.*, 2018, **442**, 403–411.

9 L. Vertuccio, S. Russo, M. Raimondo, K. Lafdi and L. Guadagno, Influence of carbon nanofillers on the curing kinetics of epoxy-amine resin, *RSC Adv.*, 2015, **5**(110), 90437–90450.

10 B. Zhou, Y. Li, G. Zheng, K. Dai, C. Liu, Y. Ma, J. Zhang, N. Wang, C. Shen and Z. Guo, Continuously fabricated transparent conductive polycarbonate/carbon nanotube nanocomposite films for switchable thermochromic applications, *J. Mater. Chem. C*, 2018, **6**(31), 8360–8371.

11 F. Zhang, W. Jiang, X. Song, J. Kang, Y. Cao and M. Xiang, Effects of Hyperbranched Polyester-Modified Carbon Nanotubes on the Crystallization Kinetics of Polylactic Acid, *ACS Omega*, 2021, **6**(15), 10362–10370.

12 Y. Yu, F. Zeng, J. Chen, J. Kang, F. Yang, Y. Cao and M. Xiang, Effects of ordered structure on non-isothermal crystallization kinetics and subsequent melting behavior of β-nucleated isotactic polypropylene/graphene oxide composites, *J. Therm. Anal. Calorim.*, 2019, **136**, 1667–1678.

13 Y. Yu, R. Xu, J. Chen, J. Kang, M. Xiang, Y. Li, L. Li and X. Sheng, Ordered structure effects on β-nucleated isotactic polypropylene/graphene oxide composites with different thermal histories, *RSC Adv.*, 2019, **9**(34), 19630–19640.

14 Y. Yu, F. Zeng, J. Chen, J. Kang, F. Yang, Y. Cao and M. Xiang, Regulating polycrystalline behavior of the β-nucleated isotactic polypropylene/graphene oxide composites by melt memory effect, *Polym. Compos.*, 2018, **40**(S1), E440–E448.

15 Y. Yu, F. Zeng, J. Chen, J. Kang, F. Yang, Y. Cao and M. Xiang, Isothermal Crystallization Kinetics and Subsequent Melting Behavior of β-Nucleated Isotactic Polypropylene/Graphene Oxide Composites with Different Ordered Structure, *Polym. Int.*, 2018, **67**(9), 1212–1220.

16 L. Li, Z. Zeng, H. Zou and M. Liang, Curing characteristics of an epoxy resin in the presence of functional graphite oxide with amine-rich surface, *Thermochim. Acta*, 2015, **614**, 76–84.

17 S. H. Ryu, J. H. Sin and A. M. Shanmugharaj, Study on the effect of hexamethylene diamine functionalized graphene

oxide on the curing kinetics of epoxy nanocomposites, *Eur. Polym. J.*, 2014, **52**, 88–97.

18 T. Kuilla, S. Bhadra, D. Yao, N. Kim, S. Bose and J. Lee, Recent advances in graphene based polymer composites, *Prog. Polym. Sci.*, 2010, **35**(11), 1350–1375.

19 J. Abenojar, M. Martínez, F. Velasco, V. Pascual-Sánchez and J. Martín-Martínez, Effect of boron carbide filler on the curing and mechanical properties of an epoxy resin, *J. Adhes.*, 2009, **85**(4–5), 216–238.

20 Y. Zhao and D. Drummer, Influence of filler content and filler size on the curing kinetics of an epoxy resin, *Polymers*, 2019, **11**(11), 1797.

21 J. Bae, J. Jang and S. H. Yoon, Cure Behavior of the Liquid-Crystalline Epoxy/Carbon Nanotube System and the Effect of Surface Treatment of Carbon Fillers on Cure Reaction, *Macromol. Chem. Phys.*, 2002, **203**(15), 2196–2204.

22 H. Xie, B. Liu, Q. Sun, Z. Yuan, J. Shen and R. Cheng, The influence of vapor-grown carbon fibers on the cure reaction of epoxy and the curing kinetics of the composites, *Acta Polym. Sin.*, 2005, (6), 891–895.

23 T. Liu, D. Chen, Y. Cao, F. Yang, J. Chen, J. Kang, R. Xu and M. Xiang, Construction of a composite microporous polyethylene membrane with enhanced fouling resistance for water treatment, *J. Membr. Sci.*, 2021, **618**, 118679.

24 R. Xu, J. Wang, D. Chen, T. Liu, Z. Zheng, F. Yang, J. Chen, J. Kang, Y. Cao and M. Xiang, Preparation and performance of a charge-mosaic nanofiltration membrane with novel salt concentration sensitivity for the separation of salts and dyes, *J. Membr. Sci.*, 2020, **595**, 117472.

25 B. Xiong, R. Chen, F. Zeng, J. Kang and Y. Men, Thermal shrinkage and microscopic shutdown mechanism of polypropylene separator for lithium-ion battery: in situ ultra-small angle X-ray scattering study, *J. Membr. Sci.*, 2018, **545**, 213–220.

26 J. Wang, R. Xu, F. Yang, J. Kang, Y. Cao and M. Xiang, Probing influences of support layer on the morphology of polyamide selective layer of thin film composite membrane, *J. Membr. Sci.*, 2018, **556**, 374–383.

27 J. Kang, D. Chen, B. Xiong, N. Zheng, F. Yang, M. Xiang and Z. Zheng, A facile route for the fabrication of polypropylene separators for lithium ion batteries with high elongation and strong puncture resistance, *Ind. Eng. Chem. Res.*, 2019, **58**(51), 23135–23142.

28 Y. Yu, B. Xiong, F. Zeng, R. Xu, F. Yang, J. Kang, M. Xiang, L. Li, X. Sheng and Z. Hao, Influences of Compression on the Mechanical Behavior and Electrochemical Performances of Separators for Lithium Ion Batteries, *Ind. Eng. Chem. Res.*, 2018, **57**(50), 17142–17151.

29 Q. Zhang, H. Peng, J. Kang, Y. Cao and M. Xiang, Effects of melt structure on non-isothermal crystallization behavior of isotactic polypropylene nucleated with α/β compounded nucleating agents, *Polym. Eng. Sci.*, 2017, **57**(9), 989–997.

30 J. Kang, F. Yang, J. Chen, Y. Cao and M. Xiang, Influences of molecular weight on the non-isothermal crystallization and melting behavior of β-nucleated isotactic polypropylene with different melt structures, *Polym. Bull.*, 2017, **74**(5), 1461–1482.

31 J. Wang, S. Zhang, Q. Liu, S. Du, Y. C. Guo, N. Zheng and F. Y. Wang, Conditional Uncorrelation and Efficient Subset Selection in Sparse Regression, *IEEE Trans. Cybern.*, 2021, 1–10.

32 J. Wang, N. Zheng, B. Chen, P. Chen, S. Chen, Z. Liu, F. Wang and B. Xi, Multivariate Correlation Entropy and Law Discovery in Large Data Sets, *IEEE Intell. Syst.*, 2018, **33**(5), 47–54.

33 R. Xu, G. Xu, J. Wang, J. Chen, F. Yang, J. Kang and M. Xiang, Influence of l-lysine on the permeation and antifouling performance of polyamide thin film composite reverse osmosis membranes, *RSC Adv.*, 2018, **8**(44), 25236–25247.

34 R. Xu, J. Wang, D. Chen, F. Yang, J. Kang, M. Xiang, L. Li and X. Sheng, Preparation of pH-responsive asymmetric polysulfone ultrafiltration membranes with enhanced anti-fouling properties and performance by incorporating poly(2-ethyl-2-oxazoline) additive, *RSC Adv.*, 2018, **8**(72), 41270–41279.

35 J. Kang, G. Weng, Z. Chen, J. Chen, Y. Cao, F. Yang and M. Xiang, New understanding in the influence of melt structure and β-nucleating agents on the polymorphic behavior of isotactic polypropylene, *RSC Adv.*, 2014, **56**(4), 29514–29526.

36 J. Kang, J. Chen, Y. Cao and H. Li, Effects of ultrasound on the conformation and crystallization behavior of isotactic polypropylene and [beta]-isotactic polypropylene, *Polymer*, 2010, **51**(1), 249–256.

37 C. Ma, L. Peng, Y. Feng, J. Shen, Z. Xiao, K. Cai, Y. Yu, Y. Min and A. J. Epstein, Polyfurfuryl alcohol spheres template synthesis of 3D porous graphene for high-performance supercapacitor application, *Synth. Met.*, 2016, **220**, 227–235.

38 S. Stankovich, D. A. Dikin, R. D. Piner, K. A. Kohlhaas, A. Kleinhammes, Y. Jia, Y. Wu, S. T. Nguyen and R. S. Ruoff, Synthesis of graphene-based nanosheets via chemical reduction of exfoliated graphite oxide, *Carbon*, 2007, **45**(7), 1558–1565.

39 D. A. Nguyen, Y. R. Lee, A. V. Raghu, H. M. Jeong, C. M. Shin and B. K. Kim, Morphological and physical properties of a thermoplastic polyurethane reinforced with functionalized graphene sheet, *Polym. Int.*, 2009, **58**(4), 412–417.

40 S.-Y. Yang, W.-N. Lin, Y.-L. Huang, H.-W. Tien, J.-Y. Wang, C.-C. M. Ma, S.-M. Li and Y.-S. Wang, Synergetic effects of graphene platelets and carbon nanotubes on the mechanical and thermal properties of epoxy composites, *Carbon*, 2011, **49**(3), 793–803.

41 X. Wang, J. Jin and M. Song, Cyanate ester resin/graphene nanocomposite: curing dynamics and network formation, *Eur. Polym. J.*, 2012, **48**(6), 1034–1041.

42 M. Huskić, S. Bolka, A. Vesel, M. Mozetič, A. Anžlovar, A. Vizintin and E. Žagar, One-step surface modification of graphene oxide and influence of its particle size on the properties of graphene oxide/epoxy resin nanocomposites, *Eur. Polym. J.*, 2018, **101**, 211–217.

43 B. A. Rozenberg, Kinetics, thermodynamics and mechanism of reactions of epoxy oligomers with amines, *Epoxy resins and composites II*, 1986, pp. 113–165.

44 H. Xie, B. Liu, Z. Yuan, J. Shen and R. Cheng, Cure kinetics of carbon nanotube/tetrafunctional epoxy nanocomposites by isothermal differential scanning calorimetry, *J. Polym. Sci. Pol. Phys.*, 2004, **42**(20), 3701–3712.

45 H. Xie, B. Liu, Q. Sun, Z. Yuan, J. Shen and R. Cheng, Cure kinetic study of carbon nanofibers/epoxy composites by isothermal DSC, *J. Appl. Polym. Sci.*, 2005, **96**(2), 329–335.

46 X. Wang, J. Jin, M. Song and Y. Lin, Effect of graphene oxide sheet size on the curing kinetics and thermal stability of epoxy resins, *Mater. Res. Express*, 2016, **3**(10), 105303.

47 X. He, J. Wang, N. Ramdani, W. Liu, L. Liu and L. Yang, Investigation of synthesis, thermal properties and curing kinetics of fluorene diamine-based benzoxazine by using two curing kinetic methods, *Thermochim. Acta*, 2013, **564**, 51–58.

48 X. He, J. Wang, Y. Wang, C. Liu, W. Liu and L. Yang, Synthesis, thermal properties and curing kinetics of fluorene diamine-based benzoxazine containing ester groups, *Eur. Polym. J.*, 2013, **49**(9), 2759–2768.

49 H. E. Kissinger, Reaction kinetics in differential thermal analysis, *Anal. Chem.*, 1957, **29**(11), 1702–1706.

50 S. Vyazovkin, A. K. Burnham, J. M. Criado, L. A. Pérez-Maqueda, C. Popescu and N. Sbirrazzuoli, ICTAC Kinetics Committee recommendations for performing kinetic computations on thermal analysis data, *Thermochim. Acta*, 2011, **520**(1–2), 1–19.

51 R. L. Blaine and H. E. Kissinger, Homer Kissinger and the Kissinger equation, *Thermochim. Acta*, 2012, **540**, 1–6.

52 C. S. Wang and C. H. Lin, Novel phosphorus-containing epoxy resins. Part II: curing kinetics, *Polymer*, 2000, **41**(24), 8579–8586.

53 H.-W. Cui, K. Suganuma and H. Uchida, Using the Ozawa method to study the thermally initiated curing kinetics of vinyl ester resin, *RSC Adv.*, 2015, **5**(4), 2677–2683.

54 J. Wu, J. Guo, Q. Zhang, L. Gao, H. Li, H. Deng, W. Jiang, G. Sui and X. Yang, Effect of different amino functionalized carbon nanotubes on curing behavior and mechanical properties of carbon fiber/epoxy composites, *Polym. Compos.*, 2018, **39**(S2), E733–E744.

55 T. Tsafack, J. M. Alred, K. E. Wise, B. Jensen, E. Siochi and B. I. Yakobson, Exploring the interface between single-walled carbon nanotubes and epoxy resin, *Carbon*, 2016, **105**, 600–606.

56 K. Yang, M. Gu and Y. Jin, Cure behavior and thermal stability analysis of multiwalled carbon nanotube/epoxy resin nanocomposites, *J. Appl. Polym. Sci.*, 2008, **110**(5), 2980–2988.

57 A. Moroni, J. Mijovic, E. M. Pearce and C. C. Foun, Cure kinetics of epoxy resins and aromatic diamines, *J. Appl. Polym. Sci.*, 1986, **32**(2), 3761–3773.

58 N. Sbirrazzuoli, A. Mititelu-Mija, L. Vincent and C. Alzina, Isoconversional kinetic analysis of stoichiometric and off-stoichiometric epoxy-amine cures, *Thermochim. Acta*, 2006, **447**(2), 167–177.